Towards a physics-based modelling of the electro-mechanical coupling in EAPs

Noy Cohen[1,2], Andreas Menzel[2,3] and Gal deBotton[1,4]

[1]Dept. of Mechanical Engineering, Ben-Gurion University, Beer-Sheva 84105, Israel;

[2]Institute of Mechanics, Dept. of Mechanical Engineering, TU Dortmund, D-44227 Dortmund, Germany;

[3]Division of Solid Mechanics, Lund University, P.O.Box 118, SE-22100 Lund, Sweden;

[4]Dept. of Biomedical Engineering, Ben-Gurion University, Beer-Sheva 84105, Israel;

Abstract

Due to the increasing number of industrial applications of electro-active polymers (EAPs), there is a growing need for electromechanical models which accurately capture their behavior. To this end, we compare the predicted behavior of EAPs undergoing homogenous deformations according to three electromechanical models. The first model is a continuum based model composed of the mechanical Gent model and a linear relationship between the electric field and the polarization. The electrical and the mechanical responses according to the second model are based on the polymer microstructure, whereas the third model incorporates a neo-Hookean mechanical response and a microstructural based long-chains model for the electrical behavior. In the microstructural motivated models the integration from the microscopic to the macroscopic levels is accomplished by the micro-sphere technique. Four types of homogenous boundary conditions are considered and the behaviors determined according to the three models are compared. The differences between the predictions of the models are discussed, highlighting the need for an in-depth investigation of the relations between the structure and the behaviors of the EAPs at microscopic level and their overall macroscopic response.

Keywords: dielectrics, EAPs, electromechanical coupling, multi-scale analysis

Author for correspondence: N. Cohen, e-mail: noyco@post.bgu.ac.il

1 Introduction

Dielectric elastomers (DEs) are materials that deform under electrostatic excitation. Due to their light weight, flexibility and availability these materials can be used in a wide variety of applications such as artificial muscles [1], energy-harvesting devices [2, 3], micropumps [4], and tunable wave guides [5, 6], among others. The principle of the actuation is based on the attraction between two oppositely charged electrodes attached to the faces of a thin soft elastomer sheet. Due to Poisson's effect, the sheet expands in the transverse direction. Toupin [7], in his theoretical work, found that this electromechanical coupling is characterized by a quadratic dependence on the applied electric field. This was later verified experimentally by Kofod et al. [8]. However, DEs have a low energy-density in comparison with other actuators such as piezoelectrics and shape memory alloys [1]. Furthermore, their feasibility is limited due to the high electric fields ($\sim 100\,\mathrm{MV/m}$) required for a meaningful actuation as a result of the relatively low ratio between the dielectric and elastic moduli [9, 10]. Specifically, common flexible polymers have low dielectric moduli while polymers with high dielectric moduli are usually stiff. Nevertheless, a few recent works suggest that this ratio may be improved. Huang et al. [11] demonstrated experimentally that organic composite EAPs (electro-active polymers) experience more than 8% actuation strain in response to an activation field of $20\,\mathrm{MV/m}$. The experimental work of Stoyanov et al. [12] showed that the actuation can be dramatically improved by embedding conducting particles in a soft polymer. In parallel, theoretical works dealing with the enhancement of coupling in composites also hint at the possibility of improved actuation with an appropriate adjustment of their microstructure [5, 13, 14, 15, 16].

The above findings motivate an in-depth multiscale analysis of the electromechanical coupling in elastic dielectrics which is inherent from their microstructure. In this work we consider the class of polymer dielectrics. A polymer is a hierarchical structure of polymer chains each of which is a long string of repeating monomers. We start by analyzing the behavior of a single monomer in a chain. Next, the response of a chain is obtained by a first level integration from the single-monomer level to the chain level. Finally, the macroscopic behavior of the polymer is obtained by a higher level summation over all chains. In this work, we utilize existing constitutive models for the chains and concentrate on the higher level summation from the chain level to the macroscopic-continuum level. To this end the physically motivated micro-sphere technique, that enables to extend one dimensional models to three dimensional models by appropriate integration over the orientation space, is exploited [17, 18]. Accordingly, this method lends itself to the characterization of polymer networks since the single chain is often treated as a 1-D object which is aligned along the chain's end-to-end vector [19, 20].

The response of a polymer subjected to purely mechanical loadings was extensively investigated at all length scales. A *macroscopic level* analysis and models describing the behavior of soft materials undergoing large deformation, such as polymers, were developed by Ogden

[21]. The *microscopic level* analysis of Kuhn and Grün [22] yielded a Langevin based constitutive relation and paved the way to various multiscale models such as the 3-chain model [23], the tetrahedral model [24, 25] and the 8-chain model [26]. Corresponding micro-sphere implementation of the Langevin model was carried out by Miehe et al. [19].

The electric response of dielectrics to electrostatic excitation was examined by Tiersten [27] and Hutter et al. [28], among others, macroscopically as well as through their microstructure. Starting with the examination of a single charge under an electric field, the relations between the different electric macroscopic quantities, such as the electric displacement, the electric field and the polarization, and microscopic quantities, such as the free and bound charge densities and the dipoles were defined and analyzed.

The study of the response of dielectrics to a coupled electromechanical loading initiated with the pioneering work of Toupin [7], who performed a theoretical analysis at the *macroscopic level.* Later on, an invariant-based representation for the constitutive behavior of EAPs was introduced by Dorfmann and Ogden [29]. Subsequently, Ask et al. [30, 31], Gei et al. [5] and Jiménez and McMeeking [32] investigated the possible influence of the deformation and its rate on the electromechanical coupling. Thylander et al. [20] made use of a corresponding micro-sphere technique at the chain level. By employing macroscopic constitutive models for the mechanical and the electrical behavior of the polymer chains, a few boundary value problems were solved by means of the numerical implementation of the micro-sphere technique and the finite element method. Initial multiscale analyses of the electromechanical response were performed by Cohen and deBotton [33, 34]. The present work focuses on the implementation of different electromechanical models to EAPs experiencing homogenous deformations under various types of boundary conditions and examination of their predicted response.

We begin this work with the detailed description of the different macroscopic and microscopic models and the presentation of the micro-sphere framework. Next, the micro-sphere technique is used to compute the macroscopic behavior of dielectrics with randomly oriented and uniformly distributed dipoles experiencing the macroscopic rotation. In section 4 we determine and compare the behavior of a polymer according to three electromechanical models under different boundary conditions. The conclusions are gathered in section 5.

2 Theoretical background

Consider the deformation of a hyperelastic dielectric body subjected to electro-mechanical loading from a referential configuration to a current one. In the reference configuration, the body occupies a region $V_0 \in \mathbb{R}^3$ with a boundary ∂V_0. The referential location of a material point is $\mathbf{X}$. In the current configuration, the body occupies a region $V \in \mathbb{R}^3$ with a boundary ∂V, and we denote the location of a material point by $\mathbf{x}$. The mapping of positions of material points from the reference to the current configurations is $\mathbf{x} = \boldsymbol{\varphi}(\mathbf{X})$, and the corresponding

deformation gradient is

$$\mathbf{F} = \nabla_{\mathbf{X}} \boldsymbol{\varphi}, \tag{1}$$

where the operation $\nabla_{\mathbf{X}}$ denotes the gradient with respect to the referential coordinate system. The right and left Cauchy-Green strain tensors are $\mathbf{C} = \mathbf{F}^T\mathbf{F}$ and $\mathbf{b} = \mathbf{F}\mathbf{F}^T$. The ratio between the volumes of an infinitesimal element in the current and the reference configurations, $J = \det\mathbf{F}$, is strictly positive. In the case of incompressible materials, which are of interest in the present work, we have $J = 1$.

The induced electric field $\mathbf{E}$ on the body satisfies the governing equation

$$\nabla_{\mathbf{x}} \times \mathbf{E} = \mathbf{0}, \tag{2}$$

in the entire space, where $\nabla_{\mathbf{x}}$ denotes the gradient with respect to the current coordinate system. Consequently, we can define a scalar field, the electric potential ϕ, such that $\mathbf{E} = -\nabla_{\mathbf{x}}\phi$. The electric displacement field is

$$\mathbf{D} = \varepsilon_0\mathbf{E} + \mathbf{P}, \tag{3}$$

where ε_0 is the permittivity of the vacuum and $\mathbf{P}$ is the polarization, or the electric dipole-density. We recall that in vacuum $\mathbf{P} = \mathbf{0}$. In the absence of free charges the electric displacement field is governed by the local equation

$$\nabla_{\mathbf{x}} \cdot \mathbf{D} = 0. \tag{4}$$

In the work of [29], the referential counterparts $\mathbf{E}^{(0)}$ and $\mathbf{D}^{(0)}$ of the electric field and the electric displacement were determined. Specifically,

$$\mathbf{E}^{(0)} = \mathbf{F}^T\mathbf{E}, \tag{5}$$

$$\mathbf{D}^{(0)} = J\mathbf{F}^{-1}\mathbf{D}, \tag{6}$$

where $\nabla_{\mathbf{X}} \times \mathbf{E}^{(0)} = \mathbf{0}$ and $\nabla_{\mathbf{X}} \cdot \mathbf{D}^{(0)} = 0$. We note that unlike $\mathbf{E}^{(0)}$ and $\mathbf{D}^{(0)}$, the referential polarization is not uniquely defined. In order to ensure that the referential polarization is energy conjugate to the referential electric field such that $\frac{1}{J}\mathbf{E}^{(0)} \cdot \mathbf{P}^{(0)} = \mathbf{E} \cdot \mathbf{P}$, we adapt the definition

$$\mathbf{P}^{(0)} = J\mathbf{F}^{-1}\mathbf{P}. \tag{7}$$

In accordance with our assumption that the dielectric solid can be treated as a hyper-elastic material, its constitutive behavior can be characterized in terms of a scalar electrical enthalpy per unit volume function W. We further assume that W can be decomposed into a mechanical and a coupled contributions, i.e. $W(\mathbf{F},\mathbf{E}) = W_0(\mathbf{F}) + W_c(\mathbf{F},\mathbf{E})$, where $W_0(\mathbf{F})$ characterizes the material response in the absence of electric excitation and $W_c(\mathbf{F},\mathbf{E})$ accounts for the difference

between W with and without electric excitation [33, 34, 35, 36]. Accordingly, the polarization is determined via

$$\mathbf{P} = -\frac{1}{J}\frac{\partial W_c}{\partial \mathbf{E}}, \tag{8}$$

and the stress developing in the material can be written as the sum

$$\boldsymbol{\sigma} = \boldsymbol{\sigma}_m + \boldsymbol{\pi} + \boldsymbol{\sigma}_v, \tag{9}$$

where

$$\boldsymbol{\sigma}_m = \frac{1}{J}\frac{\partial W(\mathbf{F})}{\partial \mathbf{F}}\mathbf{F}^T, \tag{10}$$

is the mechanical stress due to the deformation of the material,

$$\boldsymbol{\pi} = \mathbf{E} \otimes \mathbf{P}, \tag{11}$$

is the polarization stress stemming from the applied electric field in the dielectric, and

$$\boldsymbol{\sigma}_v = \varepsilon_0 \left[\mathbf{E} \otimes \mathbf{E} - \frac{1}{2}[\mathbf{E} \cdot \mathbf{E}]\mathbf{I} \right], \tag{12}$$

is the Maxwell stress in vacuum, where $\mathbf{I}$ is the second order identity tensor [35]. We emphasize that this decomposition is purely modelling-based as in an experiment the total stress can be measured, but the contributions of the individual components cannot be distinguished. In this work, we consider incompressible materials that undergo homogenous deformations and therefore a pressure like term $p\mathbf{I}$, which is determined from the boundary conditions, is added to the total stress. Assuming no body forces, the stress satisfies the local equilibrium equation

$$\nabla_{\mathbf{x}} \cdot \boldsymbol{\sigma} = \mathbf{0}. \tag{13}$$

The electrical boundary conditions are given in terms of either the electric potential or the charge per unit area ρ_a, such that $\mathbf{D} \cdot \hat{\mathbf{n}} = -\rho_a$, where $\hat{\mathbf{n}}$ is the outward pointing unit normal. Practically, in EAPs, ρ_a is the charge on the electrodes. The mechanical boundary conditions are given in terms of the displacement or the mechanical traction $\mathbf{t}$. Due to the presence of the electric field the stress in the vacuum outside of the body does not vanish. Therefore, the mechanical traction at the boundary is $[\boldsymbol{\sigma} - \boldsymbol{\sigma}_v] \cdot \hat{\mathbf{n}} = \mathbf{t}$, where the expression for $\boldsymbol{\sigma}_v$, the Maxwell stress outside the material, is given in Eq. (12) in terms of the electric field in the vacuum.

2.1 Existing models for the behavior of dielectrics

Within the framework of finite deformation elasticity the simplest constitutive model is the well-known neo-Hookean model that requires only one material parameter. The corresponding

strain energy-density function (SEDF) is

$$W_0^{nH}(\mathbf{F}) = \frac{\mu}{2}\left[I_1 - 3\right], \tag{14}$$

where μ is the shear modulus and $I_1 = \mathrm{tr}(\mathbf{C})$ is the first invariant of the right Cauchy-Green strain tensor. This model does not capture the *lock-up* effect observed in experiments and corresponds to a significant stiffening of the material at large strains. Gent [37] proposed a phenomenological constitutive model in which this effect is accounted for. The SEDF for this model

$$W_0^{G}(\mathbf{F}) = -\frac{\mu J_m}{2}\ln\left(1 - \frac{I_1 - 3}{J_m}\right), \tag{15}$$

depends on two parameters, μ and J_m. The latter is the lock-up parameter such that $J_m + 3$ is the value of I_1 at the lock-up stretch. Thus, the expression in Eq. (15) becomes unbounded at $I_1 = J_m + 3$ which captures this phenomenon.

With regard to the response of the dielectric to electrical excitation a quadratic dependence of W_c on $\mathbf{E}$ is commonly assumed, leading to the linear relation

$$\mathbf{P} = \chi\mathbf{E}, \tag{16}$$

where χ is the susceptibility of the material [38]. Consequently, the electric displacement is

$$\mathbf{D} = \varepsilon\mathbf{E}, \tag{17}$$

where $\varepsilon = \varepsilon_0 + \chi$ is the permittivity of the material. We note that this linear relation is in agreement with the invariant based representation of Dorfmann and Ogden [29]. Furthermore, an experiment carried out by Di Lillo et al. [39] on VHB 4910 showed that this assumption is fairly accurate.

Recent experiments with various types of polymers imply that the permittivity, and therefore the relation between the polarization and the electric field, is deformation dependent [40, 41, 42, 43]. A possible explanation for this dependency of the susceptibility on the deformation is related to the alteration of the inner structure of the polymer [33, 34].

In the polymer, the monomers in the chain can move or rotate relative to their neighbors thus providing the chains with a freedom to deform [44]. In order to better understand the response of polymers to an electro-mechanical loading, their microstructure should be accounted for. This can be accomplished in terms of a multiscale analysis consisting of three stages: the first involves the examination of the behavior of the monomers, the second includes analysis of the response of the chains, and the third deals with the polymer behavior at the continuum level.

Treloar [45] and Flory and Rehner [24] carried out a multiscale analysis of a polymer subjected to mechanical loading. It was assumed that the directions of the monomers, or links,

composing a chain are random, and consequently it was found that the chains are distributed according to a Gaussian distribution. Based on statistical considerations and the laws of thermodynamics, the variation in the entropy of the chain due to its deformation was determined. The overall variation in the entropy of the polymer is computed by summing the entropies of the chains. Remarkably, their result recovered the macroscopic neo-Hookean behavior. Furthermore, a comparison between the micro and macro analyses related the macroscopic shear modulus to the number of chains per unit volume N_0. Specifically, it was found that

$$\mu = kTN_0, \tag{18}$$

where k and T are the Boltzmann constant and the absolute temperature, respectively.

Due to the assumptions that lead to the use of Gaussian statistics, the lock-up effect was not captured in the above mentioned analysis. A more rigorous examination of the polymer behavior by Kuhn and Grün [22] revealed that this phenomenon is a result of the finite extensibility of the chains. According to this analysis the SEDF associated with a polymer chain is

$$W_0^{LC} = kTn_l \left[\mathscr{L}^{-1}\left(\frac{r}{n_l l}\right) \frac{r}{n_l l} + \ln\left(\frac{\mathscr{L}^{-1}\left(\frac{r}{n_l l}\right)}{\sinh\left(\mathscr{L}^{-1}\left(\frac{r}{n_l l}\right)\right)} \right) \right], \tag{19}$$

where l is the length of a link, n_l is the number of links in a chain, r is the distance between the two ends of the chain, and $\mathscr{L}^{-1}(\bullet)$ is the inverse of the Langevin function

$$\mathscr{L}(\beta) \equiv \coth(\beta) - \frac{1}{\beta} = \frac{r}{n_l l}. \tag{20}$$

Assuming that all chains undergo the macroscopic deformation, i.e. $\mathbf{r} = \mathbf{F}\mathbf{r}_0$ where $\mathbf{r}$ and $\mathbf{r}_0$ are the current and referential end-to-end vectors, respectively, the stress associated with a chain is derived from Eq. (19),

$$\boldsymbol{\sigma}_m^{LC} = kT\sqrt{n_l}\,\frac{r_0}{r}\,\mathscr{L}^{-1}\left(\frac{r}{n_l l}\right) \mathbf{F}\hat{\mathbf{r}}_0 \otimes \mathbf{F}\hat{\mathbf{r}}_0, \tag{21}$$

where $\hat{\mathbf{r}}_0$ is a unit vector in the direction of $\mathbf{r}_0$ and Eq. (10) is used. Here,

$$r_0 = l\sqrt{n_l}, \tag{22}$$

is the average length of the referential end-to-end vectors [44, 46]. The quantity $\frac{r}{n_l l} \leq 1$ describes the ratio between the end-to-end and the contour lengths of the chain, and from Eq. (22) it follows that

$$\frac{r}{n_l l} = \sqrt{\mathbf{F}\hat{\mathbf{r}}_0 \cdot \mathbf{F}\hat{\mathbf{r}}_0}\,\frac{r_0}{n_l l} = \sqrt{\mathbf{F}\hat{\mathbf{r}}_0 \cdot \mathbf{F}\hat{\mathbf{r}}_0}\,\frac{1}{\sqrt{n_l}}. \tag{23}$$

It can be shown that the limit $\frac{r}{n_l l} \to 1$ results in $\mathscr{L}^{-1}\left(\frac{r}{n_l l}\right) \to \infty$, thus capturing the experimentally observed lock-up phenomenon. The lock-up stretch is associated with the chain undergoing the largest extension such that the stretch ratio of its end-to-end vector is

$$\lambda_{max} = \sqrt{n_l}. \tag{24}$$

It is important to note that the first term in the Taylor series expansion of Eq. (21) about $\frac{r}{n_l l} = 0$ reproduces the Gaussian model [22, 46].

A few works proposed models that consider specific finite networks of chains. The 3-chain model by Wang and Guth [23] examines a network of 3 chains which are located along the axis of the principal directions of the deformation gradient. Flory and Rehner [24] and Treloar [25] proposed a network of four chains that are linked together at the center of a regular tetrahedron, and their other ends are located at the vertices of the tetrahedron. The tetrahedron deforms according to the macroscopic deformation while the chains experience different stretches. In the model proposed by Arruda and Boyce [26], 8 representative chains in specific directions relative to the principal system of the macroscopic deformation gradient are used to determine the macroscopic behavior. An anisotropic worm-like chain model in which no inherent alignment between the chosen and the principal coordinate systems is assumed was considered by Kuhl et al. [47].

A multiscale level analysis of the response of polymers with Gaussian distribution to electromechanical loading was carried out by Cohen and deBotton [33]. In this study, the changes in the magnitudes of the dipolar monomers due to the applied electric field and their rearrangement due to the mechanical deformation were accounted for. Following a model described in Stockmayer [48], Cohen and deBotton [34] considered the class of uniaxial dipoles in which the dipole is aligned with the line segment between the two contact points of a monomer to its neighbors. Thus, taking $\hat{\boldsymbol{\xi}}$ to be the unit vector along this line segment the dipole moment of a monomer is

$$\mathbf{m}_u = \mathfrak{K}\left[\hat{\boldsymbol{\xi}} \otimes \hat{\boldsymbol{\xi}}\right]\mathbf{E}, \tag{25}$$

where $\mathfrak{K}$ is a material constant. The dipole of a chain composed of n_d uniaxial dipoles with an end-to-end vector in the direction $\hat{\mathbf{r}}$ is [33]

$$\mathbf{m}_c \approx \frac{\mathfrak{K} n_d}{3}\left[\mathbf{I} + \frac{16}{3\pi^2}\left[\frac{r}{n_d l}\right]\left[\mathbf{I} - 3\hat{\mathbf{r}} \otimes \hat{\mathbf{r}}\right]\right]\mathbf{E}. \tag{26}$$

If we assume that all chains undergo the macroscopic deformation, then $\hat{\mathbf{r}} = \frac{\mathbf{F}\mathbf{r}_0}{\sqrt{[\mathbf{F}\mathbf{r}_0]\cdot[\mathbf{F}\mathbf{r}_0]}}$. In accordance with a second type of dipoles discussed in Stockmayer [48], Cohen and deBotton [34] proposed an expression for a transversely isotropic (TI) dipole, where the dipole is aligned

with the projection of the electric field on the plane perpendicular to $\hat{\boldsymbol{\xi}}$,

$$\mathbf{m}_t = \frac{\mathfrak{K}}{2}\left[\mathbf{I} - \hat{\boldsymbol{\xi}} \otimes \hat{\boldsymbol{\xi}}\right]\mathbf{E}. \tag{27}$$

An expression for the dipole of a chain made out of transversely isotropic dipoles is determined by following the steps followed in the derivation of Eq. (26) for the uniaxial dipoles.

The resulting polarization of the polymer is determined by summing the dipoles of the chain in a representative volume element of a volume V^R via [38]

$$\mathbf{P} = \frac{1}{V^R}\sum_i \mathbf{m}_c, \tag{28}$$

and the resulting polarization stress is computed via Eq. (11).

2.2 The micro-sphere technique

Consider a unit sphere whose surface represents the directions of the referential end-to-end vectors. The directional averaging of a quantity $\bullet$ over the unit sphere can be approximated with a discrete summation

$$\langle \bullet \rangle = \frac{1}{4\pi}\int_A \bullet \, \mathrm{d}A \approx \sum_{i=1}^{m} \bullet^{(i)} w^{(i)}, \tag{29}$$

where the index $i = 1, ..., m$ refers to a unit direction vector $\hat{\mathbf{r}}_0^{(i)}$ where $\bullet^{(i)}$ is the value of quantity $\bullet$ in the direction $\hat{\mathbf{r}}_0^{(i)}$ and $w^{(i)}$ is an appropriate non-negative weight function constrained by $\Sigma_{i=1}^{m} w_i = 1$ [17, 19, 49]. In general, Eq. (29) can be combined with a more general anisotropic distribution function [50, 51].

In the case of polymers the vectors $\hat{\mathbf{r}}_0^{(i)}$ represent the directions of the end-to-end vectors of the polymer chains or, from a numerical point of view, the integration directions in orientation space. For randomly and isotropically oriented chains, or rather isotropic integration schemes, the vectors $\hat{\mathbf{r}}_0^{(i)}$ satisfy

$$\sum_{i=1}^{m} \hat{\mathbf{r}}_0^{(i)} w^{(i)} = \mathbf{0}, \tag{30}$$

and

$$\sum_{i=1}^{m} \hat{\mathbf{r}}_0^{(i)} \otimes \hat{\mathbf{r}}_0^{(i)} w^{(i)} = \frac{1}{3}\mathbf{I}. \tag{31}$$

In view of Eqs. (30) and (31) the micro-sphere technique naturally lends itself to the calculation of the macroscopic polarization and stress. Specifically, for a polymer with chains composed of n_d dipoles and N_0 chains per unit referential volume, Eq. (28) may be written as

$$\mathbf{P} = \frac{N_0}{J}\left\langle \mathbf{m}_c \right\rangle, \tag{32}$$

and the macroscopic stress according to Eq. (21) as

$$\boldsymbol{\sigma}_m^L = \frac{N_0}{J}\left\langle \boldsymbol{\sigma}_m^{LC} \right\rangle, \tag{33}$$

where we use the notation suggested in Eq. (29).

Bažant and Oh [17] demonstrated that a specific choice of 42 directions guarantees sufficient accuracy for the application discussed in their work. We follow this conjecture where the integration directions and the corresponding weight functions are given in Table 1 of Bažant and Oh [17]. We note that other integration schemes are available, as demonstrated by Waffenschmidt et al. [52], Ostwald et al. [53] and the references cited therein.

3 Dielectrics with randomly distributed monomers

Consider a model of a dielectric composed of n_0 monomers per unit referential volume, which are treated as mechanical rods and electric dipoles. The dielectric is subjected to a mechanical deformation, locally represented by $\mathbf{F}$, and an electric field $\mathbf{E}$. We assume that the electric field induced on a monomer by its neighbors is small in comparison with the applied electric field [34]. We examine first a dielectric with uniaxial monomers, the behavior of which is governed by the quadratic form in Eq. (25). If all of the dipoles experience the macroscopic rotation, i.e. $\hat{\boldsymbol{\xi}} = \mathbf{R}\hat{\boldsymbol{\xi}}_0$ where $\mathbf{R} = \mathbf{F}\mathbf{C}^{-1/2}$ is a proper rotational tensor, then the polarization according to Eq. (32) is

$$\mathbf{P} = n_0 \langle \mathbf{m}_c \rangle = n_0 \mathfrak{K} \mathbf{R} \sum_{i=1}^{42} \hat{\boldsymbol{\xi}}_0^{(i)} \otimes \hat{\boldsymbol{\xi}}_0^{(i)} w^{(i)} \mathbf{R}^T \mathbf{E} = \frac{n_0 \mathfrak{K}}{3} \mathbf{E}, \tag{34}$$

where Eqs. (29) and (31) are used. The corresponding polarization stress is

$$\boldsymbol{\pi} = \mathbf{E} \otimes \mathbf{P} = \frac{n_0 \mathfrak{K}}{3} \mathbf{E} \otimes \mathbf{E}. \tag{35}$$

In the case of a dielectric composed of n_0 TI dipolar monomers per unit referential volume, cf. Eq. (27), which mechanically act as rigid rods, the same assumptions that led to Eq. (34) lead to

$$\mathbf{P} = n_0 \langle \mathbf{m}_c \rangle = n_0 \frac{\mathfrak{K}}{2} \sum_{i=1}^{42} \left[\mathbf{I} - \mathbf{R}\hat{\boldsymbol{\xi}}_0^{(i)} \otimes \hat{\boldsymbol{\xi}}_0^{(i)} \mathbf{R}^T \right] w^{(i)} \mathbf{E} = \frac{n_0 \mathfrak{K}}{3} \mathbf{E}. \tag{36}$$

Accordingly, the expression for the polarization stress is given in Eq. (35). We note that the polarization and polarization stress calculated in Eqs. (34), (36) and (35) are identical to the exact expressions obtained by Cohen and deBotton [34].

4 Dielectric elastomers

We examine the behaviors of incompressible dielectric elastomers according to three different models under various homogenous electromechanical loading conditions and compare between their predicted responses. To facilitate the comparison we assume that in the limit of infinitesimal deformations and small electric excitations all three models admit the same behavior. Specifically we assume that the initial shear modulus and electric susceptibility are $\mu = 0.1\,\mathrm{MPa}$ and $\chi = 3\,\varepsilon_0$. In those models in which the lock-up effect is accounted for we choose the model parameters such that under purely mechanical biaxial loading the lock-up stretch is $\lambda^{lu} = 5$. The precise models and the numerical values assumed for their parameters are as follows:

1. The *macroscopic* model - the mechanical behavior is characterized by the Gent model (15) with the aforementioned shear modulus and $J_m = 47$. The electric behavior is determined according to the linear model (17) with the initial permittivity $\varepsilon = 4\,\varepsilon_0$.

2. The *microscopic* model - the Langevin model (21) is utilized in order to describe the mechanical behavior, where $n_l = 25$ is chosen to fit the assumed lock-up stretch according to Eq. (24) and $N_0 = \frac{\mu}{kT}$. We employ the long-chains model (26) with chains that are composed of $n_d = 100$ uniaxial dipoles (Eq. 25) to characterize the dielectric response of the polymer. The material constant $\mathfrak{K}$ is chosen such that $\frac{\mathfrak{K} N_0 n_d}{3} = 3\,\varepsilon_0$ to ensure that the referential polarization is identical to the one admitted by the macroscopic model.

3. The *Gaussian* model - the neo-Hookean model (14) with (18) are used, where $N_0 = \frac{\mu}{kT}$, in conjunction with the long-chains model (26) to characterize the mechanical and the electrical behaviors, respectively. We assume that a chain is composed of $n_d = 100$ uniaxial dipoles (Eq. 25), where the chosen long-chains model constant is identical to the one determined for the microscopic model.

In the following, we examine a thin layer of a polymer whose opposite faces are covered with flexible electrodes with negligible stiffness. The electrodes are charged with opposite charges so that the difference in the electric potential induces an electric field across the layer. From a mechanical point of view we consider four boundary conditions. In the first two cases different displacements are prescribed at the boundary and consequently the deformation gradient is defined. In the following two representative cases we set the traction on the boundaries. We choose a cartesian coordinate system in which the referential electric field is aligned with the $\hat{\mathbf{y}}$-axis and calculate the macroscopic polarization according to the microscopic and the Gaussian models via Eq. (32). The polarization stress is computed according to Eq. (11). The mechanical stress is computed via Eqs. (15), (14) and (21) for the macroscopic, the Gaussian and

the microscopic models, respectively. The pressure term is determined from the traction free boundaries to which the electrodes are attached and subsequently the total stress is computed via Eq. (9).

For convenience we define the dimensionless normal stress along the $\hat{\mathbf{x}}$-axis $\bar{\sigma} = \frac{1}{\mu}\hat{\mathbf{x}}\cdot\boldsymbol{\sigma}\hat{\mathbf{x}}$ and the dimensionless referential electric field and referential electric displacement along the $\hat{\mathbf{y}}$-direction $\bar{E}^{(0)} = \sqrt{\frac{\varepsilon}{\mu}}\mathbf{E}^{(0)}\cdot\hat{\mathbf{y}}$ and $\bar{D}^{(0)} = \frac{1}{\sqrt{\varepsilon\mu}}\mathbf{D}^{(0)}\cdot\hat{\mathbf{y}}$, respectively. In the following examples the current configuration counterparts of $\bar{E}^{(0)}$ and $\bar{D}^{(0)}$ are $\bar{E} = \sqrt{\frac{\varepsilon}{\mu}}\mathbf{E}\cdot\hat{\mathbf{y}}$ and $\bar{D} = \frac{1}{\sqrt{\varepsilon\mu}}\mathbf{D}\cdot\hat{\mathbf{y}}$, respectively, as follows from Eqs. (5) and (6).

4.1 Equibiaxial stretching perpendicular to the electric field

In this case the material is stretched along the axes $\hat{\mathbf{x}}$ and $\hat{\mathbf{z}}$ such that $\lambda_x = \lambda_z = \lambda$. As stated previously, the $\hat{\mathbf{y}}$-axis is aligned with the referential electric field and due to the assumed incompressibility $\lambda_y = \frac{1}{\lambda^2}$. This setting is common in various experiments with EAPs [40, 41, 42, 43].

Figs. (1a) and (1b) depict $\bar{\sigma}$ and $\bar{D}$ as functions of λ^2 and $\bar{E}$, respectively. The curves with the squared marks correspond to the macroscopic model, the curves with the hollow circle marks to the Gaussian model, and the curves with the filled circle marks to the microscopic model. The applied referential electric field is $E^{(0)} = 50\,\frac{\mathrm{MV}}{\mathrm{m}}$. We point out that at $\lambda^2 = 1$ the dimensionless stress according to the three models is not zero but very small. Fig. (1a) illustrates the stress increase at the lock-up stretch according to the macroscopic and the microscopic models. As expected, this effect is not observed when the Gaussian model is employed. Furthermore, since the electric field tends to stretch the material in the transverse plane, as long as the prescribed stretch is smaller than the electrically induced stretch, the overall stress is compressive. We emphasize that since the potential is held fixed, as the layer is stretched the current electric field increases and hence also the electromechanically induced stress. This gives rise to different types of loss of stability phenomena which are outside the scope of the current work. The reader is referred to the works by, e.g., Rudykh et al. [15], Dorfmann and Ogden [54], Bertoldi and Gei [55] and Shmuel et al. [6]. Only when the prescribed stretches are large enough, the total stress becomes tensile.

In Fig. (1b) we observe a linear dependence of the electric displacement on the electric field according to the macroscopic model, as follows from Eq. (17) and the assumed constant permittivity. Since the graph is plotted in terms of the dimensionless quantities its slope is unity. In contrast, the Gaussian and the microscopic models predict a stronger than linear increase in the electric displacement as we stretch the material. This is a result of the predicted increase in the permittivity due to the stretching of a polymer with chains made up of uniaxial dipoles

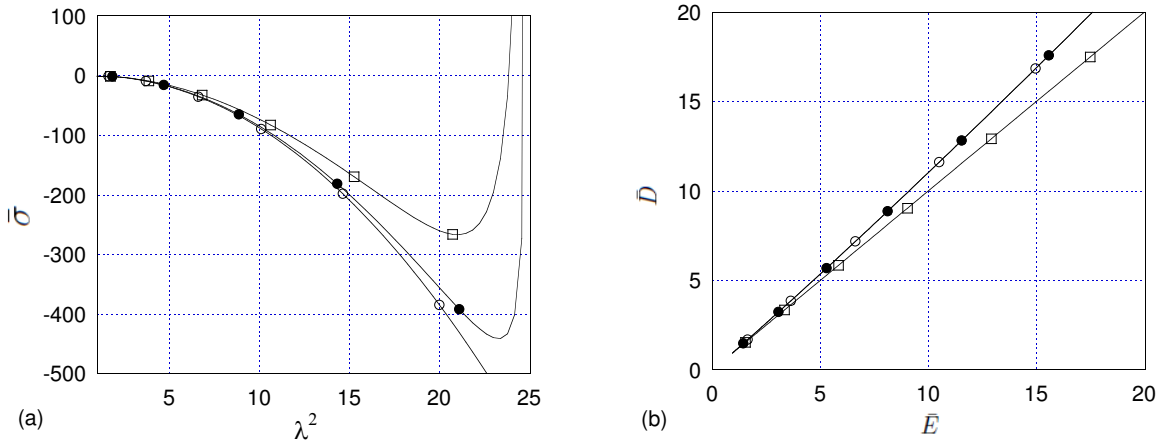

Figure 1: The dimensionless stress $\bar{\sigma}$ (a) and electric displacement $\bar{D}$ (b) versus the stretch of the transverse plane and the dimensionless electric field according to the macroscopic model (the curve with the square marks), the Gaussian model (the curve with the hollow circle marks) and the microscopic model (the curve with the filled circle marks).

[33].

4.2 Pure shear deformation in the plane of the electric field

Once again we analyze a thin layer of a polymer whose opposite faces are covered with flexible electrodes with negligible stiffness. As before the $\hat{\mathbf{y}}$-axis is aligned with the electric field, but in this case the deformation of the material along the $\hat{\mathbf{z}}$-axis is constraint such that $\lambda_z = 1$. The layer is stretched along the $\hat{\mathbf{x}}$-axis such that $\lambda_x = \lambda$ and the incompressibility condition yields $\lambda_y = \frac{1}{\lambda}$.

Fig. (2a) depicts the dimensionless normal stress that develops along the $\hat{\mathbf{x}}$-axis as a function of the stretch according to the macroscopic model (the curve with the square marks), the Gaussian model (the curve with the hollow circle marks) and the microscopic model (the curve with the filled circle marks) under the applied referential electric field $E^{(0)} = 100\,\frac{\mathrm{MV}}{\mathrm{m}}$. The inability of the neo-Hookean model to capture the lock-up stretch is again clearly depicted. We also notice that there is a difference between the lock-up stretches predicted by the macroscopic and the microscopic models. This is because the lock-up stretch according to the Langevin model is determined by the maximum eigenvalue of the deformation gradient as seen from Eq. (24), whereas according to the Gent model it depends on the first invariant of the right Cauchy-Green strain tensor. Treloar [46] presented experimental results demonstrating that polymers lock-up at different values under different types of deformations, and therefore we conclude that in this aspect the Gent model may be a better predictor. We wish to point out that the lock-up stretch according to the microscopically motivated 8-chain model of Arruda and Boyce [26], in which the chain behaves according to Eq. (21), depends on I_1 as well and is able to capture the different lock-up stretch values under various states of deformation. A

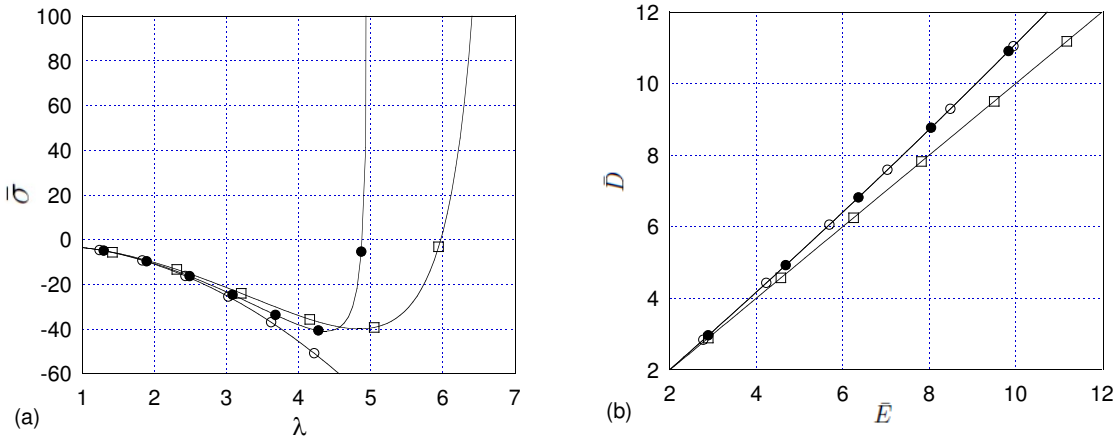

Figure 2: The dimensionless stress $\bar{\sigma}$ (a) and electric displacement $\bar{D}$ (b) versus the axial stretch and the dimensionless electric field according to the macroscopic model (the curve with the square marks), the Gaussian model (the curve with the hollow circle marks) and the microscopic model (the curve with the filled circle marks).

comparison of different models and their calibration according to the data reported by Treloar [46] was carried out by Steinmann et al. [56].

The curves with the square, hollow and filled circle marks in Fig. (2b) correspond to the macroscopic model, the Gaussian model and the microscopic model, respectively. Here, the dependency of $\bar{D}$ on $\bar{E}$ is illustrated. Due to the constant permittivity, we again note the linear dependency predicted by the macroscopic model. The Gaussian and the microscopic models, which are based on the electric long-chains model, predict a change in the permittivity as a result of the mechanical stretch, in agreement with the experimental findings of Choi et al. [40], Wissler and Mazza [41], McKay et al. [42], Qiang et al. [43]. Since the deformation is dictated by the boundary condition, the Gaussian and the microscopic models predict the same electric behavior.

4.3 Equibiaxial actuation normal to the electric field

We once again examine a thin layer of a polymer whose opposite faces are covered with flexible electrodes with negligible stiffness. This time, however, the circumferential boundary of the layer is traction free, thus allowing the layer to expand in the plane transverse to the direction of the electric field in response to the electric excitation. We choose the same system of axes as in subsection 4.1 and, thanks to the symmetry of the loading, the deformation gradient is diagonal with $\lambda_x = \lambda_z = \lambda$. Due to the assumed incompressibility we have $\lambda_y = \frac{1}{\lambda^2}$.

Fig. (3a) displays the dimensionless referential electric field $\bar{E}^{(0)}$ as a function of the induced stretch of the transverse plane according to the macroscopic model (the curve with the square marks), the Gaussian model (the curve with the hollow circle marks) and the microscopic model (the curve with the filled circle marks). The loss of stability discussed in the

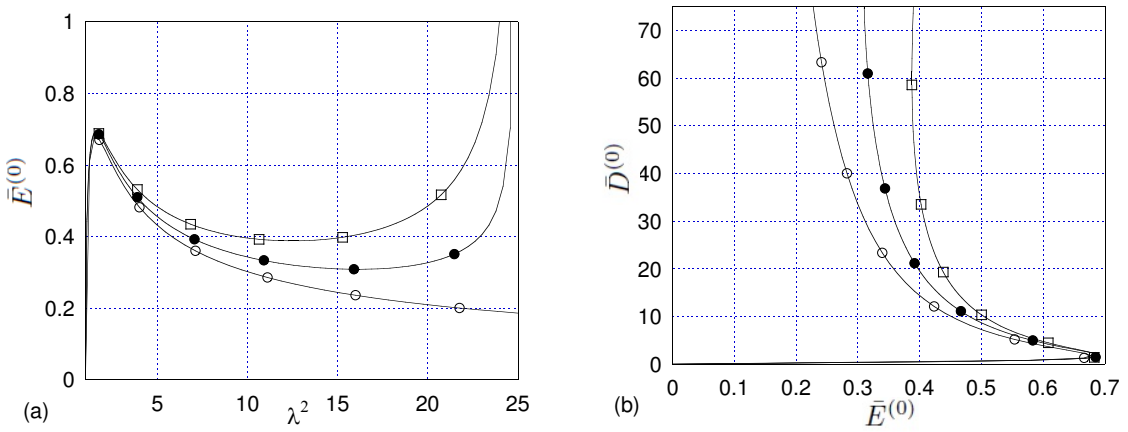

Figure 3: The dimensionless referential electric field $\bar{E}^{(0)}$ (a) and electric displacement $\bar{D}^{(0)}$ (b) versus the stretch of the transverse plane and the dimensionless referential electric field according to the macroscopic model (the curve with the square marks), the Gaussian model (the curve with the hollow circle marks) and the microscopic model (the curve with the filled circle marks).

works of Dorfmann and Ogden [54], Bertoldi and Gei [55], Rudykh and deBotton [57] and Shmuel et al. [6] is demonstrated again. We note that after the peak at $\bar{E}^{(0)} \approx 0.7$, even though the current electric field increases monotonically, the Gaussian model predicts a decrease in the referential electric field with an increase of the stretch. In an experiment where the referential electric field is controlled, the macroscopic and microscopic models predict a jump in the planar stretch. This effect of a transition between two states is known as snap-through (58; 4).

The curves with the square, hollow and filled circle marks in Fig. (3b) correspond to the macroscopic, the Gaussian and the microscopic models, where the predicted dependencies of $\bar{D}^{(0)}$ on $\bar{E}^{(0)}$ in the direction of the electric field are depicted. Essentially, this plot illustrates the amount of charge per unit referential surface area as a function of the potential difference divided by the initial thickness of the layer. Initially, we observe an increase of the surface charge with an increase of the electric potential. However, beyond the peak at $\bar{E}^{(0)} \approx 0.7$ there is a reversed trend where, at equilibrium, the electric potential drops while the surface charge increases. This occurs in conjunction with the uncontrollable increase in the area of the actuator as shown in Fig. (3a). From a practical viewpoint this implies that beyond the peak, in a manner reminiscent of an electrical short-circuit, excessive current flows from the system electric source while the electric potential drops. We stress that due to the thinning of the layer the current electric field increases and may result in a failure of the DE due to electric breakdown. We also note that even though the same electric model is used in both the Gaussian and the microscopic models, there is a difference in the relations between the electric field and the electric displacement. This is due to the different mechanical deformations resulting from

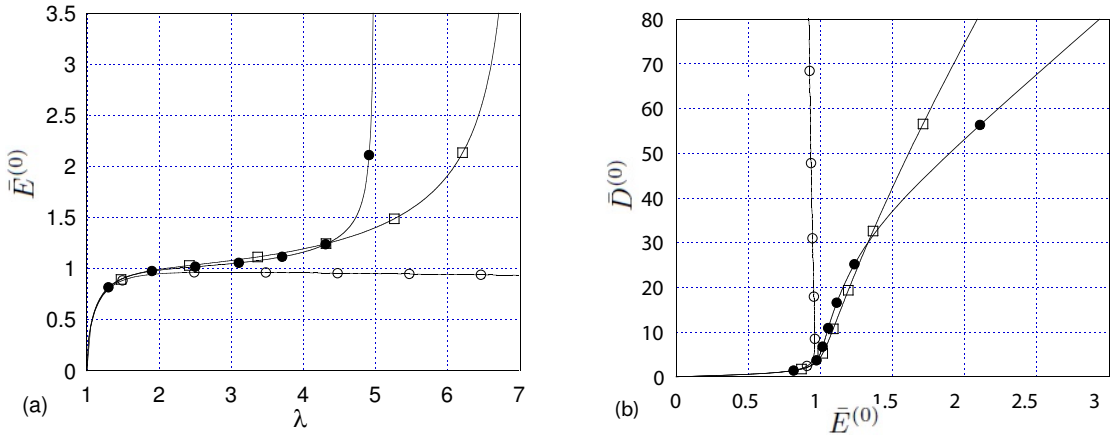

Figure 4: The dimensionless referential electric field $\bar{E}^{(0)}$ (a) and electric displacement $\bar{D}^{(0)}$ (b) versus the stretch and the dimensionless referential electric field according to the macroscopic model (the curve with the square marks), the Gaussian model (the curve with the hollow circle marks) and the microscopic model (the curve with the filled circle marks).

the applied electric field according to the two different models.

4.4 Uniaxial actuation normal to the electric field

We consider a setting reminiscent of the one considered in subsection 4.3, but this time the layer is free to expand only along the $\hat{\mathbf{x}}$-direction. Consequently, the deformation gradient components are $\lambda_z = 1$, $\lambda_x = \lambda$, and $\lambda_y = \frac{1}{\lambda}$.

Fig. (4a) shows the dimensionless referential electric field as a function of the stretch according to the macroscopic model (the curve with the square marks), the Gaussian model (the curve with the hollow circle marks) and the microscopic model (the curve with the filled circle marks). As mentioned previously, the predicted lock up stretches are $\lambda^{lu} = 5$ and $\lambda^{lu} \approx 7$ according to the microscopic and the macroscopic models, respectively. Unlike the biaxial case described in subsection 4.3, this loading does not admit loss of stability according to the macroscopic and the microscopic models. The Gaussian model, that is based on the mechanical neo-Hookean model, reaches a peak at $\bar{E}^{(0)} \approx 1$ and then monotonically decreases.

Fig. (4b) depicts the dependence of $\bar{D}^{(0)}$ on $\bar{E}^{(0)}$. According to the Gaussian model, represented by the curve with the hollow circle marks, no significant changes in the surface charge are observed as we initially increase the electric potential difference. However, beyond the peak of $\bar{E}^{(0)} \approx 1$, this model predicts an unstable behavior as a result of the electrical long-chains model. In order to maintain equilibrium according to the macroscopic and the microscopic models an increase in the charge on the electrodes requires an increase in the voltage difference between them. Thus, the Gaussian model is admitting a behavior that is qualitatively

different from the behaviors of the other two models.

5 Concluding remarks

We determined the behavior of an incompressible polymer undergoing homogenous deformations according to three electromechanical models under four types of boundary conditions. The first model incorporates well-known macroscopically motivated constitutive relations for the mechanical and the electrical behaviors. The second, microscopic model, combines mechanical and electrical models stemming from the microstructure of the polymer. The third model assumes a Gaussian distribution of the polymer chains and accordingly the mechanical and the electrical behaviors are determined. We comment that the material parameters n_d and n_l, which denote the number of dipoles and links, respectively, are used as fitting parameters and therefore the electrical long-chains model and the Langevin model are not consistent. Further investigations in this regard is needed.

In the first two representative examples we apply a referential electric field by setting the potential difference between the electrodes and controlling the deformation. In the following two examples we apply a referential electric field and set the traction on the boundaries of the polymer. In order to determine the polarization and the stress resulting according to the microscopic models we make use of the micro-sphere technique. A comparison between the results shows that the macroscopically and the microscopically motivated models predict different behaviors. Therefore, this work encourages a further and a more rigorous investigation into the connection between the two scales aimed at deepening our understanding of the micro-macro relations and the mechanisms which control the actuation. Moreover, analysis of this type may open the path to the design and manufacturing of polymers with microstructures that enable to improve the electromechanical coupling.

Competing interests

We have no competing interests.

Authors' contributions

All authors carried out the research and the analysis jointly and N.C. was responsible for the programming. All authors gave final approval for publication.

Funding

The first author would like to thank the financial assistance of the Minerva Foundation. Additionally, partial financial support for this work was provided by the Swedish Research Council (Vetenskapsrï¿œdet) under grant 2011-5428, and is gratefully acknowledged by the second author. Lastly, the first and the last authors wish to acknowledge the support of the Israel Science Foundation founded by the Israel Academy of Sciences and Humanities (grant 1246/11).

References

[1] Y. Bar-Cohen. EAP history, current status, and infrastructure. In Y. Bar-Cohen, editor, *Electroactive Polymer (EAP) Actuators as Artificial Muscles*, chapter 1, pages 3–44. SPIE press, Bellingham, WA, 2001.

[2] T. McKay, B. O'Brien, E. Calius, and L. Anderson. An integrated, self-priming dielectric elastomer generator. *Applied Physics Letters*, 97:062911, 2010.

[3] R. Springhetti, E. Bortot, G. deBotton, and M. Gei. Optimal energy-harvesting cycles for load-driven dielectric generators in plane strain. *IMA Journal of Applied Mathematics*, 79(5):929–946, 2014.

[4] S. Rudykh, K. Bhattacharya, and G. deBotton. Snap-through actuation of thick-wall electroactive balloons. *International Journal of Non-linear Mechanics*, 47:206–209, 2012.

[5] M. Gei, R. Springhetti, and E. Bortot. Performance of soft dielectric laminated composites. *Smart Materials and Structures*, 22(10):104014, 2013.

[6] G. Shmuel, M. Gei, and G. deBotton. The rayleigh-lamb wave propagation in dielectric elastomer layers subjected to large deformations. *International Journal of Non-Linear Mechanics*, 47(2):307 – 316, 2012. Nonlinear Continuum Theories.

[7] R. A. Toupin. The elastic dielectric. *Journal of Rational Mechanics and Analysis*, 5: 849–915, 1956.

[8] G. Kofod, P. Sommer-Larsen, R. Kornbluh, and R. Pelrine. Actuation response of polyacrylate dielectric elastomers. *Journal of Intelligent Material Systems and Structures*, 14: 787–793, 2003.

[9] R. Pelrine, R. Kornbluh, J. Joseph, R. Heydt, Q. Pei, and S. Chiba. High-field deformation of elastomeric dielectrics for actuators. *Materials Science and Engineering: C*, 11(2):89 – 100, 2000.

[10] R. Pelrine, R. Kornbluh, Q. Pei, and J. Joseph. High-speed electrically actuated elastomers with strain greater than 100%. *Science*, 287(5454):836–839, 2000.

[11] C. Huang, Q. M. Zhang, G. deBotton, and K. Bhattacharya. All-organic dielectric-percolative three-component composite materials with high electromechanical response. *Applied Physics Letters*, 84:4391–4393, 2004.

[12] H. Stoyanov, M. Kollosche, D. N. McCarthy, and G. Kofod. Molecular composites with enhanced energy density for electroactive polymers. *Journal of Materials Chemistry*, 20: 7558–7564, 2010.

[13] L. Tian, L. Tevet-Deree, G. deBotton, and K. Bhattacharya. Dielectric elastomer composites. *Journal of the Mechanics and Physics of Solids*, 60(1):181 – 198, 2012.

[14] E. Galipeau and P. Ponte Castañeda. The effect of particle shape and distribution on the macroscopic behavior of magnetoelastic composites. *International Journal of Solids and Structures*, 49(1):1 – 17, 2012.

[15] S. Rudykh, A. Lewinstein, G. Uner, and G. deBotton. Analysis of microstructural induced enhancement of electromechanical coupling in soft dielectrics. *Applied Physics Letters*, 102(15):–, 2013.

[16] O. Lopez-Pamies. Elastic dielectric composites: Theory and application to particle-filled ideal dielectrics. *Journal of the Mechanics and Physics of Solids*, 64:61–82, 2014.

[17] P. Bažant and B.H. Oh. Efficient numerical integration on the surface of a sphere. *ZAMM-Journal of Applied Mathematics and Mechanics/Zeitschrift für Angewandte Mathematik und Mechanik*, 66(1):37–49, 1986.

[18] I. Carol, M. Jirasek, and Z. P. Bažant. A framework for microplane models at large strain, with application to hyperelasticity. *International Journal of Solids and Structures*, 41(2): 511 – 557, 2004.

[19] C. Miehe, S. Göktepe, and F. Lulei. A micro-macro approach to rubber-like materials–part i: the non-affine micro-sphere model of rubber elasticity. *Journal of the Mechanics and Physics of Solids*, 52(11):2617 – 2660, 2004.

[20] S. Thylander, A. Menzel, and M. Ristinmaa. An electromechanically coupled microsphere framework: application to the finite element analysis of electrostrictive polymers. *Smart Materials and Structures*, 21(9):094008, 2012.

[21] R. W. Ogden. *Non-Linear Elastic Deformations*. Dover Publications, New York, 1997.

[22] W. Kuhn and F. Grün. Beziehungen zwischen elastischen konstanten und dehnungsdoppelbrechung hochelastischer stoffe. *Kolloid-Zeitschrift*, 101(3):248–271, 1942.

[23] M. C. Wang and E. Guth. Statistical theory of networks of non-gaussian flexible chains. *The Journal of Chemical Physics*, 20:1144–1157, 1952.

[24] P. J. Flory and J. Rehner. Statistical mechanics of cross-linked polymer networks i. rubberlike elasticity. *The Journal of Chemical Physics*, 11(11):512–520, 1943.

[25] L. R. G. Treloar. The elasticity of a network of long-chain molecules.-III. *Transactions of the Faraday Society*, 42:83–94, 1946.

[26] E. M. Arruda and M. C. Boyce. A three-dimensional constitutive model for the large stretch behavior of rubber elastic materials. *Journal of the Mechanics and Physics of Solids*, 41:389–412, 1993.

[27] H. F. Tiersten. *A Development of the Equations of Electromagnetism in Material Continua*, volume 36 of *Springer Tracts in Natural Philosophy*. Springer-Verlag, New York, 1990.

[28] K. Hutter, A. A. F. van de Ven, and A. Ursescu. *Electromagnetic Field Matter Interactions in Thermoelasic Solids and Viscous Fluids*. Number 710 in Lecture Notes in Physics. Springer, Berlin Heidelberg, 2nd edition, 2006.

[29] A. Dorfmann and R. W. Ogden. Nonlinear electroelasticity. *Acta Mechanica*, 174:167–183, 2005.

[30] A. Ask, A. Menzel, and M. Ristinmaa. Phenomenological modeling of viscous electrostrictive polymers. *International Journal of Non-Linear Mechanics*, 47(2):156 – 165, 2012.

[31] A. Ask, A. Menzel, and M. Ristinmaa. Electrostriction in electro-viscoelastic polymers. *Mechanics of Materials*, 50(0):9 – 21, 2012.

[32] S. Jiménez and R. M. McMeeking. Deformation dependent dielectric permittivity and its effect on actuator performance and stability. *International Journal of Non-Linear Mechanics*, 57:183–191, 2013.

[33] N. Cohen and G. deBotton. The electromechanical response of polymer networks with long-chain molecules. *Mathematics and Mechanics of Solids*, 2014. doi: 10.1177/1081286514550574.

[34] N. Cohen and G. deBotton. Multiscale analysis of the electromechanical coupling in dielectric elastomers. *European Journal of Mechanics - A/Solids*, 48(0):48 – 59, 2014.

[35] R. M. McMeeking and C. M. Landis. Electrostatic forces and stored energy for deformable dielectric materials. *Journal of Applied Mechanics, Transactions ASME*, 72: 581–590, 2005.

[36] R. M. McMeeking, C. M. Landis, and S. M. A. Jimenez. A principle of virtual work for combined electrostatic and mechanical loading of materials. *International Journal of Nonlinear Mechanics*, 42(6):831–838, 2007.

[37] A. N. Gent. A new constitutive relation for rubber. *Rubber Chemistry and Technology*, 69:59–61, 1996.

[38] T. Blythe and D. Bloor. *Electrical Properties of Polymers*. Cambridge University Press, Cambridge, UK, 2 edition, 2008.

[39] L. Di Lillo, A. Schmidt, D. A. Carnelli, P. Ermanni, G. Kovacs, E. Mazza, and A. Bergamini. Measurement of insulating and dielectric properties of acrylic elastomer membranes at high electric fields. *Journal of Applied Physics*, 111(2):–, 2012.

[40] H. R. Choi, K. Jung, N. H. Chuc, M. Jung, I. Koo, J. Koo, J. Lee, J. Lee, J. Nam, M. Cho, and Y. Lee. Effects of prestrain on behavior of dielectric elastomer actuator. In *Smart Structures and Materials*, pages 283–291. International Society for Optics and Photonics, 2005.

[41] M. Wissler and E. Mazza. Electromechanical coupling in dielectric elastomer actuators. *Sensors and Actuators A: Physical*, 138(2):384–393, 2007.

[42] T. G. McKay, E. Calius, and I. A. Anderson. The dielectric constant of 3m vhb: a parameter in dispute, 2009.

[43] J. Qiang, H. Chen, and B. Li. Experimental study on the dielectric properties of polyacrylate dielectric elastomer. *Smart Materials and Structures*, 21(2):025006, 2012.

[44] P. J. Flory. *Principles of polymer chemistry*. Cornell Univ Press, Ithaca, NY, 1953.

[45] L. R. G. Treloar. The elasticity of a network of long-chain molecules. I. *Transactions of the Faraday Society*, 39:36–41, 1943.

[46] L. R. G. Treloar. *The Physics of Rubber Elasticity*. Clarendon Press, Oxford, 1975.

[47] E. Kuhl, A. Menzel, and K. Garikipati. On the convexity of transversely isotropic chain network models. *Philosophical Magazine*, 86(21-22):3241–3258, 2006.

[48] W. H. Stockmayer. Dielectric dispersion in solutions of flexible polymers. *Pure and Applied Chemistry*, 15(539):2816, 1967.

[49] A. Menzel and T. Waffenschmidt. A microsphere-based remodelling formulation for anisotropic biological tissues. *Philosophical Transactions of the Royal Society A: Mathematical, Physical and Engineering Sciences*, 367(1902):3499–3523, 2009.

[50] V. Alastrué, M.A. Martínez, M. Doblaré, and A. Menzel. Anisotropic micro-sphere-based finite elasticity applied to blood vessel modelling. *Journal of the Mechanics and Physics of Solids*, 57(1):178 – 203, 2009.

[51] V. Alastrué, M.A. Martínez, A. Menzel, and M. Doblaré. On the use of non-linear transformations for the evaluation of anisotropic rotationally symmetric directional integrals.

application to the stress analysis in fibred soft tissues. *International Journal for Numerical Methods in Engineering*, 79(4):474–504, 2009.

[52] T. Waffenschmidt, A. Menzel, and E. Kuhl. Anisotropic density growth of bone-a computational micro-sphere approach. *International Journal of Solids and Structures*, 49(14): 1928 – 1946, 2012.

[53] R. Ostwald, T. Bartel, and A. Menzel. A gibbs-energy-barrier-based computational micro-sphere model for the simulation of martensitic phase-transformations. *International Journal for Numerical Methods in Engineering*, 97(12):851–877, 2014.

[54] A. Dorfmann and R.W. Ogden. Nonlinear electroelastostatics: Incremental equations and stability. *International Journal of Engineering Science*, 48(1):1 – 14, 2010.

[55] K. Bertoldi and M. Gei. Instabilities in multilayered soft dielectrics. *Journal of the Mechanics and Physics of Solids*, 59(1):18 – 42, 2011.

[56] P. Steinmann, M. Hossain, and G. Possart. Hyperelastic models for rubber-like materials: consistent tangent operators and suitability for treloar's data. *Archive of Applied Mechanics*, 82(9):1183–1217, 2012.

[57] S. Rudykh and G. deBotton. Stability of anisotropic electroactive polymers with application to layered media. *Zeitschrift für angewandte Mathematik und Physik*, 62(6): 1131–1142, 2011.

[58] N. Goulbourne, E. Mockensturm, and M. Frecker. A nonlinear model for dielectric elastomer membranes. *Journal of Applied Mechanics*, 72(6):899–906, 2005.